ACS APPLIED MATERIALS & INTERFACES

www.acsami.org Research Article

Prediction of Bi_2Te_3-Sb_2Te_3 Interfacial Conductance and Superlattice Thermal Conductivity Using Molecular Dynamics Simulations

Prabudhya Roy Chowdhury, Jingjing Shi, Tianli Feng, and Xiulin Ruan*

Cite This: *ACS Appl. Mater. Interfaces* 2021, 13, 4636–4642 Read Online

ACCESS | Metrics & More | Article Recommendations

ABSTRACT: Bismuth telluride (Bi_2Te_3) and its alloys with antimony telluride (Sb_2Te_3) have long been considered to be the best room-temperature bulk thermoelectric (TE) materials. In recent decades, proof-of-concept demonstrations on Bi_2Te_3-Sb_2Te_3 nanostructures have shown high TE performance due to reduction in lattice thermal conductivities. Particularly, ultra-low thermal conductivities have been observed in Bi_2Te_3-Sb_2Te_3 1D superlattices, leading to thermoelectric figures of merit (ZT) as high as 2.4. In contrast, very few computational studies have been performed to provide insight into the phonon transport across these nanostructures. In this work, we use non-equilibrium molecular dynamics simulations with previously developed force fields to simulate thermal transport across Bi_2Te_3-Sb_2Te_3 interfaces and superlattices. We first calculate the thermal conductance associated with a Bi_2Te_3-Sb_2Te_3 interface across a temperature range of 200−400 K. The values are also compared with thermal conductances calculated by a modified Landauer transport formalism using phonon transmission coefficients obtained from the diffuse mismatch model. Our results show that inelastic scattering processes contribute to an increase in interfacial thermal conductance at higher temperatures. Finally, we calculate the thermal conductivities of Bi_2Te_3-Sb_2Te_3 superlattices with varying period lengths from 2 to 18 nm. A minimum thermal conductivity of 0.27 W/mK is observed at a period length of 4 nm, which is attributed to the competition between incoherent and coherent phonon transport regimes. In comparison with previous experimental measurements in the literature, our results show good agreement with respect to the range of thermal conductivity values and the period length corresponding to the minimum superlattice thermal conductivity.

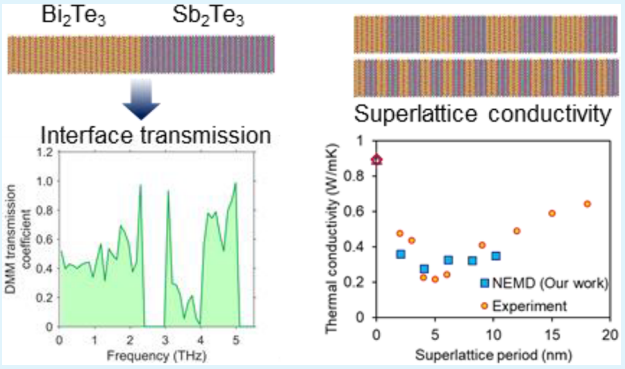

KEYWORDS: *bismuth telluride, antimony telluride, superlattice, interfacial thermal conductance, thermal conductivity, molecular dynamics*

1. INTRODUCTION

Thermoelectric energy conversion provides an attractive solution to utilize large amounts of waste heat, such as that generated by traditional fossil-fuel-based energy production systems, into electrical power directly. The performance of a thermoelectric generator can be characterized by its figure of merit (ZT), given by $ZT = S^2\sigma T/(\kappa_e + \kappa_l)$, where S, σ, and T are the Seebeck coefficient, electrical conductivity, and temperature, respectively, and κ_e and κ_l are the electronic and lattice contributions to the thermal conductivity of the material. Although various approaches exist to lower κ_l such as alloying and introduction of vacancies and defects, the difficulty in tuning ZT arises due to the coupled nature of the electrical and thermal transport properties. Bismuth telluride (Bi_2Te_3), antimony telluride (Sb_2Te_3), and their alloys have long been found to provide the highest figures of merit among bulk materials due to their low κ_l at room temperature. In recent decades, the ability to fabricate nanostructures with dimensions comparable to the mean free paths of phonons has led to successful proof-of-concept demonstrations of high ZT devices based on these materials.[1−12] In particular, binary superlattices, made of periodically alternating layers of two materials, have received widespread attention due to their ultra-low κ_l. In these structures, phonons can undergo repeated scattering at interfaces, leading to a much lower lattice thermal conductivity than the constituent materials.[1,2,12−14]

In order to expedite the search for higher efficiency systems and gain insight into the underlying transport mechanisms,

Received: October 5, 2020
Accepted: December 22, 2020
Published: January 12, 2021

https://dx.doi.org/10.1021/acsami.0c17851
ACS Appl. Mater. Interfaces 2021, 13, 4636–4642

such experimental demonstrations need to be complemented by computational studies of these systems. Moreover, results of computer simulations can also be used as the training data in informatics and machine learning methods which have become increasingly popular in performing highly accelerated design optimization of nanostructures with targeted transport properties.[15−19] Despite the long-standing importance of Bi_2Te_3 and Sb_2Te_3 as thermoelectric materials, very few modeling studies have been performed to understand thermal transport in their binary nanostructures. Pattamatta and Madnia[20] studied the thermal transport properties of Bi_2Te_3-Sb_2Te_3 1D superlattices and 2D nanowire composites using the Boltzmann transport equation (BTE). Since only the particle nature of phonon modes was considered within this approach, their results did not show the existence of a minimum thermal conductivity with respect to varying superlattice period, which is now widely understood to occur due to competing phonon wave effects. Katcho *et al.*[21] calculated the thermal conductivity of $(Bi_{1-x}Sb_x)_2Te_3$ alloys with and without embedded spherical nanoparticles. Their results showed that significant reduction in thermal conductivities of the nanoparticle-alloy composites could be achieved with nanoparticle diameters less than 10 nm. We note that the BTE approach used in these studies required the estimation of phonon mean free paths by fitting to the bulk thermal conductivities and cannot be considered completely predictive methods. In contrast, molecular dynamics (MD) simulations, which require no input fitting parameters except appropriate interatomic potentials, have been successfully used to predict thermal transport in various bulk materials and nanostructures with all orders of anharmonic phonon scattering events included inherently. As a result, MD simulations have been used to predict thermal transport in bulk Bi_2Te_3[22−24] and its nanostructures[21,25−28] as well as bulk Sb_2Te_3,[29] with close agreement to experimental measurements. In this work, we calculate the phonon transport properties across a Bi_2Te_3-Sb_2Te_3 interface and 1D superlattices with varying periods, using non-equilibrium molecular dynamics simulations. The simulation methodology including details of the multilayer structures is described in Section 2. The results for thermal conductance at the single interface and thermal conductivity of the superlattices are then presented in Section 3.

2. METHODOLOGY

2.1. Simulation Materials. Bulk bismuth telluride (Bi_2Te_3) and antimony telluride (Sb_2Te_3) both occur in quintuple layered (QL) lattice structures (Figure 1a), where each layer is composed as Te1−X−Te2−X−Te1 (X = Bi or Sb). The two Te atoms are in different bonding environments, with the Te2 atoms forming strong intralayer bonds, and the Te1 atoms forming weaker interlayer van der Waals bonds. The bulk materials can be described by the primitive rhombohedral cell containing 5 atoms or the conventional hexagonal unit cell having 15 atoms (3 QLs). The experimental hexagonal cell lattice constants of the two materials are $a_{Bi_2Te_3}$ = 4.369 Å and $c_{Bi_2Te_3}$ = 30.42 Å for Bi_2Te_3[30] and $a_{Sb_2Te_3}$ = 4.264 Å and $c_{Sb_2Te_3}$ = 30.458 Å for Sb_2Te_3.[31] In this work, orthogonal simulation domains are created using the conventional cells. A cross-section size of 10 × 14 unit cells is used in the x and y directions, which were found to provide converged thermal conductivity values. Along the z direction, the single interface and superlattice structures

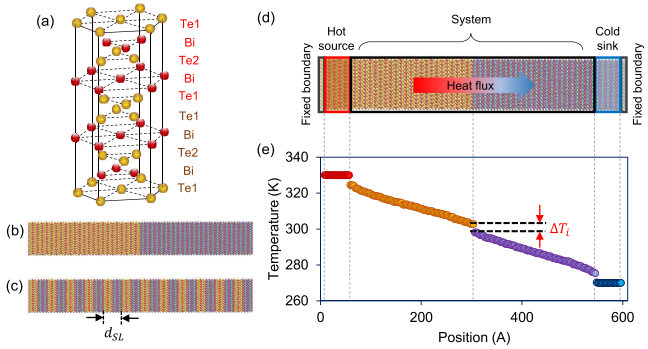

Figure 1. (a) Crystal structure of Bi_2Te_3 showing two quintuple layers. (b) Schematic of Bi_2Te_3-Sb_2Te_3 single interface and (c) superlattice with period d_{SL}. (d) NEMD simulation domain showing the fixed layers of atoms at each end, the hot and cold baths and the direction of heat flux through the system in between. (e) Representative temperature profile for the single interface structure, showing the temperature drop ΔT_i at the interface.

are created by stacking of the quintuple layers. The period lengths of the superlattices studied in our work are varied from 2 to 18 QLs (2−18 nm). The structures of the single interface and a representative superlattice are shown in Figure 1b,c.

2.2. Molecular Dynamics Simulations. To calculate the thermal transport properties in multilayer Bi_2Te_3-Sb_2Te_3 structures, non-equilibrium molecular dynamics (NEMD) are performed using the LAMMPS package.[32] The equations of motion are integrated using a velocity-Verlet algorithm with a time step of 1 fs, which is sufficient to resolve the phonon modes of both the materials. The schematic of the simulation domain is shown in Figure 1d. The Bi_2Te_3-Sb_2Te_3 system is placed between two bulk regions of atoms at either end. Initially, periodic boundary conditions are imposed in all three directions. The entire simulation domain is first relaxed under constant temperature and pressure (NPT) for 1×10^6 time steps (1 ns) to reduce the strain on the system, after which it is switched to a constant volume and energy ensemble (NVE) and run for 0.5×10^6 time steps (500 ps) for proper equilibration. Subsequently, 1 quintuple layer of atoms at each end is fixed to implement fixed boundary conditions along the z direction. Next to each of the fixed ends, a 5 QL section of atoms are thermostatted using Langevin dynamics to create and maintain a temperature gradient across the system. The thermal conductivity calculated using NEMD simulations can be dependent on the lengths of the heat reservoirs. By varying the length of the thermal reservoirs, we find that the thermal conductivity does not vary if their length is 5 QL (5 nm) or more. A temperature difference of 60 K is applied across the system through the thermostatted regions. The temperature gradient in the system is obtained by dividing the simulation domain into bins along the z direction and averaging the kinetic energies of the atoms within a bin. This temperature data is collected and averaged over 20 ns after a steady state is achieved to minimize statistical fluctuations. The time taken to observe a steady-state temperature gradient and a stable heat current within the system depends on the simulation domain length in the z direction and can vary from less than 1 ns for small systems to 5 ns for larger lengths. A representative temperature profile for the single interface structure, showing the temperature drop ΔT_i at the interface, is provided in Figure 1e. The interfacial thermal conductance (G) can be calculated

https://dx.doi.org/10.1021/acsami.0c17851
ACS Appl. Mater. Interfaces 2021, 13, 4636−4642

from the steady-state heat flux (q'') and the temperature drop as

$$G = \frac{q''}{\Delta T_i} \tag{1}$$

To calculate the thermal conductivity of the multilayer structure, a linear fit is made to the temperature profile across the system. The sections near the thermal reservoirs are excluded since they include non-linear effects due to the velocities of the reservoir atoms being artificially scaled. The slope of the linear fit is used to calculate the thermal conductivity as

$$\kappa = \frac{q''}{\mathrm{d}T/\mathrm{d}z} \tag{2}$$

Suitable classical interatomic potentials need to be specified for each material to evaluate the interatomic forces during the MD simulation. Here, we use a two-body Morse potential form to represent the short-range interactions for each material, which is given by

$$\varphi_s(r_{ij}) = D_e[\{1 - e^{-a(r_{ij}-r_0)}\} - 1] \tag{3}$$

where φ_s is the short-range interatomic potential between atoms i and j, r_{ij} is the distance between the atoms, and D_e, a, and r_0 are the Morse potential parameters. The parameters for bulk Bi_2Te_3 were fitted to this form by Qiu and Ruan[22] and have been widely used to predict thermal transport in both the bulk material[22,24] and nanostructures such as thin films,[25−27] nanowires,[28] and alloys with embedded nanoparticles.[21] Similarly, the Morse potential parameters were fitted for Sb_2Te_3 in our previous work[29] and subsequently used to predict the lattice thermal conductivity of the bulk material in good agreement with experimental measurements. We employ the above parameters in this work to describe the interactions among atoms belonging to the Bi_2Te_3 layers and Sb_2Te_3 layers, respectively. In each of these two sets of potential parameters, the cutoff radius (r_c) for interactions has been carefully chosen to preserve the layered structure of the materials.

Since no parametrization has been performed for the cross-interactions between atoms belonging to the two different materials, we need to develop suitable mixing rules to obtain the Morse potential parameters for atomic interactions at the interfaces. Here, the parameters for the cross-interactions are obtained as the arithmetic average of the parameters for similar types of interactions within each of the materials. For example, the interaction parameters between Bi in Bi_2Te_3 and Te1 in Sb_2Te_3 are obtained by averaging the parameters for the Bi−Te1 interaction in Bi_2Te_3 and Sb−Te1 in Sb_2Te_3. The cutoffs for the cross-interactions are chosen to be the same as those of the corresponding types of bonds within each of the bulk materials. The entire set of cross-interaction parameters used in this work is provided in Table 1. In addition to the short-range interactions, we use a particle−particle particle−mesh (PPPM) solver to handle the long-range coulombic forces due to the charges on the atoms. Considering the partially covalent nature of the materials, it is appropriate to assign partial charges to the atoms; the details of which can be found in earlier works.[22,29]

2.3. Modified Landauer Transport Calculation. We also calculate the thermal conductance across a single interface using the modified Landauer transport framework. For this, we consider an interface perpendicular to the z direction, between two semi-infinite bulk regions. The interfacial thermal conductance is calculated according to eq 1, where the heat flux across the interface is given by

$$q''_{1\to 2} = \frac{1}{2(2\pi)^3}\sum_i \int_{\mathbf{k}} \hbar\omega(\mathbf{k}, i)|\mathbf{v}_g(\mathbf{k}, i)\cdot\mathbf{n}| [f(\omega(\mathbf{k}, i), T_1) - f(\omega(\mathbf{k}, i), T_2)]\tau_{1\to 2}(\omega(\mathbf{k}, i))\mathrm{d}\mathbf{k} \tag{4}$$

In eq 4, $\omega(\mathbf{k}, i)$ is the frequency of the phonon mode with branch i at the k-vector $\mathbf{k}$, $\mathbf{v}_g$ is the phonon group velocity, $\mathbf{n}$ is the unit vector normal to the interface, f is the phonon occupation number given by $f(\omega, T) = 1/(e^{(\hbar\omega/k_BT)} - 1)$, and $\tau_{1\to 2}$ is the frequency-dependent phonon transmission across the interface. To account for the highly anisotropic phonon transport properties of the two bulk materials, the integration in eq 4 needs to be carried out over the full Brillouin zone (BZ). This approach was previously followed by Reddy *et al.*[33] using the Born−von Karman lattice dynamical model for obtaining phonon properties and recently by Li *et al.*[34] who used *ab initio* calculations for the full phonon dispersion. In this work, the phonon properties are obtained from lattice dynamics calculation employing the above-described interatomic potentials and performed using the General Utility Lattice Program (GULP).[35] We discretize the Brillouin zone using a 65 × 65 × 65 **k**-point grid to carry out the integration numerically. The acoustic mismatch model (AMM) and the diffuse mismatch model (DMM) are two widely used models for calculating phonon transmission coefficients across an interface considering elastic scattering only. The AMM assumes completely specular reflection at interfaces; however, considering the relatively low Debye temperatures of Bi_2Te_3 (θ_D = 164 K) and Sb_2Te_3 (θ_D = 179 K),[36] the probability of specular reflection is quite low. Here, we use the DMM to calculate the phonon transmission coefficients to compare with our NEMD results. The DMM makes the assumption that phonons incident at an interface will lose all memory of their initial state (within the constraint of elastic scattering) and can transmit to either side with a probability proportional to the number of available phonon modes in that side of the interface. As a result, the DMM transmission probability can be calculated with respect to phonon frequency only, without considering the polarizations of the incident and transmitted phonons. The DMM transmission coefficients are calculated as

Table 1. Morse Potential Parameters for Cross-Interactions between Bi_2Te_3 and Sb_2Te_3 Atoms[a]

type of interaction	D_e (eV)	a (1/Å)	r_o (Å)	r_c (Å)
Bi−Sb	0.087	2.162	4.231	5.5
Bi−Te3	0.991	1.288	3.054	4.0
Bi−Te4	0.560	1.211	3.211	4.0
Te1−Sb	0.991	1.288	3.054	4.0
Te1−Te3	0.074	1.697	3.718	5.0
Te1−Te4	0.779	0.663	4.492	5.5
Te2−Sb	0.560	1.211	3.211	4.0
Te2−Te3	0.779	0.663	4.492	5.5
Te2−Te4	0.066	2.757	4.286	5.0

[a]The Te3 and Te4 atoms belong to Sb_2Te_3 and are in similar environments as the Te1 and Te2 atoms in Bi_2Te_3, respectively.

https://dx.doi.org/10.1021/acsami.0c17851
ACS Appl. Mater. Interfaces 2021, 13, 4636−4642

$$\tau_{1\to 2}(\omega) = \frac{\Delta V_2 \sum_{k,i} |\mathbf{v}_g \cdot \mathbf{n}| \delta(\omega'(\mathbf{k}, i), \omega)}{\Delta V_1 \sum_{\mathbf{k},i} |\mathbf{v}_g \cdot \mathbf{n}| \delta(\omega', \omega) + \Delta V_2 \sum_{\mathbf{k},i} |\mathbf{v}_g \cdot \mathbf{n}| \delta(\omega', \omega)} \quad (5)$$

Here, the summations are carried out over the discretized BZs of each material using the corresponding phonon properties, ΔV_i is the volume of a discretized cell in the BZ of material i, and $\delta(\omega', \omega)$ is the Kronecker delta function, which evaluates to 1 only when $\omega'(\mathbf{k}, i) = \omega$ to ensure elastic scattering.

Recently, it has been shown by Feng *et al.*[37,38] that phonon modes on either side of an interface can be in strong thermal non-equilibrium with each other. The original Landauer formulation does not include the effect of such non-equilibrium in the phonon temperatures used to calculate the temperature drop across the interface given by

$$\Delta T = T_{e,1} - T_{e,2} \quad (6)$$

Here, $T_{e,1}$ and $T_{e,2}$ are the incident temperatures of the phonons emitted from the reservoirs in materials 1 and 2. However, the phonon temperature on side 1(2) of the interface is governed by the presence of incident and reflected phonons in material 1(2) as well as transmitted phonons from material 2(1). Considering the temperature of all these types of phonons, Shi *et al.*[39] proposed a modal non-equilibrium Landauer method using modal effective temperatures $T_{\lambda,1}$ and $T_{\lambda,2}$, where

$$T_{\lambda,1} = T_{e,1} - \tau_{\lambda,1\to 2}(T_{e,1} - T_{e,2})/2 \quad (7)$$

$$T_{\lambda,2} = T_{e,2} + (1 - \tau_{\lambda,1\to 2})(T_{e,1} - T_{e,2})/2 \quad (8)$$

Using these modified temperatures in the interface temperature drop as $\Delta T_\lambda = T_{\lambda,1} - T_{\lambda,2}$, the authors were able to show much better agreement of the calculated G with experimental results. More importantly, their approach was able to resolve the failure of the original Landauer formulation wherein a finite interfacial resistance is obtained even for an imaginary interface within a bulk material. As a result, we use the modified effective equilibrium temperatures in our Landauer transport calculations.

3. RESULTS AND DISCUSSION

3.1. Thermal Conductance across a Single Interface.

We first study the phonon transport across the Bi_2Te_3-Sb_2Te_3 single interface. The atomic configurations, lattice constants and, thus, the phonon properties of the two bulk materials are very similar to each other. Figure 2a shows the phonon dispersions in the two bulk materials along the high symmetry $\Gamma - Z$ direction (cross-plane), obtained from lattice dynamics calculations. The acoustic phonon branches and the lower optical phonon branches are very well matched in both materials, which points to a high phonon transmission across the interface. Since the simple two-body form of the developed interatomic potentials is not well suited for accurately reproducing the higher optical phonon branches, we ignore the mismatch at higher frequencies. Moreover, the contribution of optical phonons to the thermal conductivities of the bulk materials was found to be low from previous molecular dynamics simulation studies.[22,23,29] The phonon density of states (PDOS) over the entire BZ for the two materials is also shown in Figure 2b. As seen in the figure, the low frequency

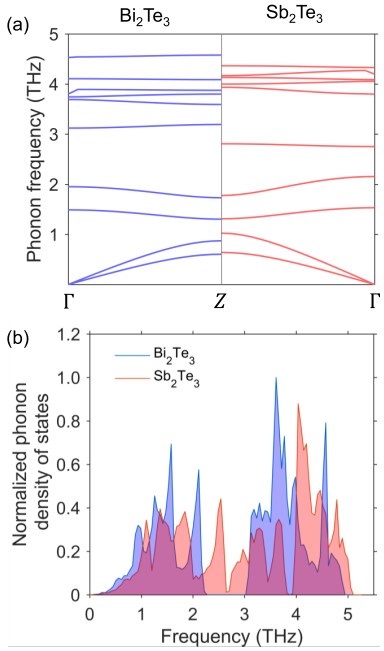

Figure 2. (a) Phonon dispersion along the $\Gamma - Z$ (cross-plane) direction in bulk Bi_2Te_3 (left) and bulk Sb_2Te_3 (right). (b) Phonon density of states in bulk Bi_2Te_3 (blue) and bulk Sb_2Te_3 (red).

portions of the PDOS are very well matched with respect to the position and magnitude of the dominant peaks.

Next, NEMD simulations are performed to calculate the thermal conductance across the Bi_2Te_3-Sb_2Te_3 interface for interface temperatures ranging from 200 to 400 K. The results are shown in Figure 2a. The thermal conductance value increases from 90 to 130 MW/m^{2}K with an increase in temperature, indicating the greater ease of thermal transport at higher temperatures. At low temperatures, the phonon transmission across the interface is largely expected to be elastic in nature, which places a constraint on the number of available phonon modes on the other side to receive thermal energy. With an increase in temperature, the increase in inelastic scattering allows transfer of energy to a larger number of phonon modes with different frequencies due to three, four, and higher-order anharmonic phonon scattering processes. This is in good agreement with previous computational studies highlighting the role of anharmonic phonon processes in interfacial thermal transport.[28,40−43] Moreover, due to the relatively large difference in the acoustic and optical branches of both Bi_2Te_3 and Sb_2Te_3, the occurrence of inelastic scattering processes at room temperature and higher temperatures is expected to be quite significant.

In order to gain insight into the spectral dependence of interfacial transport, we compute the phonon transmission coefficients using the DMM (Figure 3(b)). The DMM transmission coefficient is around 0.40 − 0.45 for frequencies less than 1 THz, which can be correlated to the highly matched PDOS and group velocities at these lower frequencies. The interfacial thermal conductance obtained using the modified Landauer transport calculations and DMM transmission coefficients is plotted in Figure 3a for comparison with the NEMD calculated conductances. The DMM conductance increases with temperature and saturates at a value of 75 MW/m^{2}K over temperatures of 40 K. The difference between the DMM conductance and the NEMD conductance increases

https://dx.doi.org/10.1021/acsami.0c17851
ACS Appl. Mater. Interfaces 2021, 13, 4636−4642

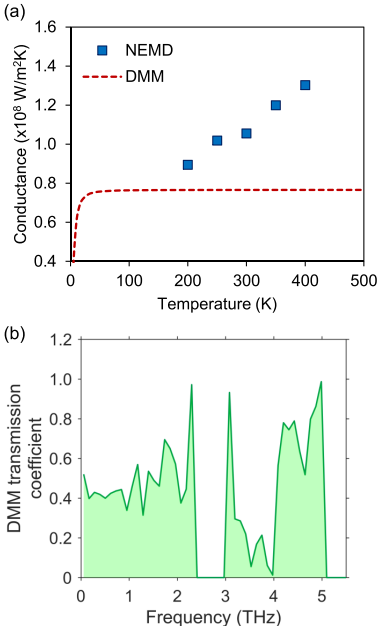

Figure 3. (a) Variation of thermal conductance of Bi_2Te_3-Sb_2Te_3 interface with temperature, calculated using NEMD simulations (solid boxes) and the modified Landauer approach with DMM transmission coefficients (dashed line). (b) Phonon transmission coefficients from Bi_2Te_3 to bulk Sb_2Te_3 calculated using the DMM.

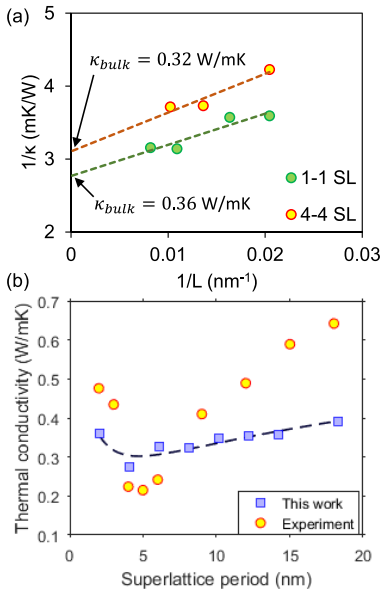

Figure 4. (a) Variation of $1/\kappa$ with $1/L$ for the 1-1 and 4-4 Bi_2Te_3-Sb_2Te_3 SLs and the bulk thermal conductivity calculated by extrapolating the linear fit to infinite length. (b) Variation of the *N*-*N* Bi_2Te_3-Sb_2Te_3 SL κ with the SL period calculated using NEMD simulations (blue squares). Experimental data by Venkatasubramanian[2] are plotted for comparison (yellow circles).

with increasing temperature, which is attributed to the increase in pathways for energy transfer between the phonons by inelastic scattering processes.

3.2. Thermal Conductivity of Superlattices. NEMD simulations are also used to calculate the thermal conductivities of the *N*-*N* superlattice system with varying superlattice period, where *N* refers to the number of quintuple layers of Bi_2Te_3 and Sb_2Te_3 within a period. The thermal conductivity calculated using NEMD simulations is dependent on the length of the system across which the non-equilibrium conditions are maintained. Insufficiently large NEMD domain sizes can cause phonons from one reservoir to reach the other without scattering and also lead to artificial effects due to phonon reflection at the reservoirs. Schelling *et al.*[44] proposed a formulation to correlate the system length L to the limited phonon mean free path λ, given by $\lambda^{-1} = \lambda_\infty^{-1} + L^{-1}$, where λ_∞ is the intrinsic phonon mean free path. From this, it follows that a linear relation between the inverse of thermal conductivity and the inverse of system length can be expected. The bulk thermal conductivity can then be obtained by extrapolating the linear curve to infinite length. Figure 4a shows the calculation of bulk thermal conductivity from the extrapolated linear fits for the 1-1 and 4-4 SLs.

The variation of the superlattice thermal conductivity with respect to the SL period is shown in Figure 4b. The thermal conductivity initially decreases with increasing superlattice period length and reaches a minimum of 0.27 W/mK at a period length of 4 nm. With a further increase in superlattice period, the thermal conductivity increases. Several experimental[2,45−48] and numerical[49−56] studies have highlighted the existence of a minimum superlattice thermal conductivity in 1D and 2D periodic systems as the period length is varied, which has been attributed to the competition between incoherent phonon and coherent phonon dominated transport regimes. At large superlattice period lengths, the thermal transport is mainly limited by incoherent phonon scattering at the interfaces, which increases at lower superlattice period lengths or higher interface densities. In this regime, anharmonic phonon−phonon scattering leads to loss of phase information before the phonons encounter an interface. If the period length is reduced further such that phonons encounter an interface before anharmonic phonon scattering occurs, interference of phonons undergoing phase-preserved reflections at the interfaces leads to a modified phonon spectrum. These coherent phonons are not scattered at the interfaces, and the thermal conductivity actually increases at very low superlattice period lengths, which has been explained by mechanisms such as less zone folding leading to weaker band flattening and increased group velocities.

The thermal conductivities of Bi_2Te_3-Sb_2Te_3 SLs were experimentally measured by Venkatasubramanian[2] using a thin film 3-ω method. Their data is plotted in Figure 4b for comparison with our NEMD calculations. The experimental data shows a larger variation in thermal conductivity (0.22 − 0.64 W/mK) than our NEMD results (0.27 − 0.39 W/mK) for the range of superlattice period lengths considered in our calculations. Overall, we find that our calculated values lie in the same range as the experimental results and exhibit similar trends. Moreover, the observed minimum κ_l in our results occurs around the same superlattice period length as the experimental data. The discrepancies between experimental and calculated results can partly arise from difficulties in fabricating superlattices with nanometer-scale period lengths, which can lead to the presence of atomic interdiffusion at the interfaces and variance in the superlattice period thicknesses.

4. CONCLUSIONS

In summary, we have performed calculations of thermal transport across Bi_2Te_3-Sb_2Te_3 interfaces and superlattices using non-equilibrium molecular dynamics (NEMD) simu-

https://dx.doi.org/10.1021/acsami.0c17851
ACS Appl. Mater. Interfaces 2021, 13, 4636−4642

lations. The NEMD simulations employ the two-body interatomic Morse potential parameters developed in our earlier works, which can accurately reproduce thermal transport properties in the bulk materials and nanostructures. We also used a modified Landauer transport formalism to calculate the interfacial thermal conductance, with the phonon transmission coefficients obtained from the diffuse mismatch model (DMM). Our calculations utilize the phonon dispersion over the full Brillouin zone to account for the anisotropic thermal transport properties of the bulk materials. The highly matched nature of the acoustic phonons and the lower optical phonon branches are reflected in the DMM transmission coefficients at low frequencies. We observe a significant difference between the thermal conductances calculated using NEMD and the Landauer transport calculations at higher temperatures, which is attributed to the increasing contribution of inelastic phonon−phonon scattering processes not captured by the DMM. We also used NEMD simulations to calculate the thermal conductivities of Bi_2Te_3-Sb_2Te_3 superlattices (SLs) with varying period lengths. A minimum SL thermal conductivity of 0.27 W/mK is observed at a period length of 4 nm from our NEMD calculations. Our results show good agreement with experimental measurements found in the literature with respect to the range of thermal conductivities and the period length of the minimum SL thermal conductivity. The insight gained in our study paves the way for designing efficient thermoelectric materials and incorporating other phonon scattering mechanisms such as atomic diffusion at interfaces and randomness in SL layer thicknesses.

AUTHOR INFORMATION

Corresponding Author

Xiulin Ruan − *School of Mechanical Engineering and the Birck Nanotechnology Center, Purdue University, West Lafayette, Indiana 47907-2088, United States;* orcid.org/0000-0001-7611-7449; Email: ruan@purdue.edu

Authors

Prabudhya Roy Chowdhury − *School of Mechanical Engineering and the Birck Nanotechnology Center, Purdue University, West Lafayette, Indiana 47907-2088, United States;* orcid.org/0000-0002-2708-983X

Jingjing Shi − *George W. Woodruff School of Mechanical Engineering, Georgia Institute of Technology, Atlanta, Georgia 30332, United States*

Tianli Feng − *Buildings and Transportation Science Division, Oak Ridge National Laboratory, Oak Ridge, Tennessee 37831, United States;* orcid.org/0000-0002-7284-5657

Complete contact information is available at: https://pubs.acs.org/10.1021/acsami.0c17851

Notes

The authors declare no competing financial interest.

ACKNOWLEDGMENTS

This work was supported by the Defence Advanced Research Projects Agency (award no. HR0011-15-2-0037) and the School of Mechanical Engineering, Purdue University. Simulations were performed at the Rosen Center of Advanced Computing at Purdue University. T.F. acknowledges the Professional Development Funding from Oak Ridge National Laboratory.

REFERENCES

(1) Venkatasubramanian, R.; Siivola, E.; Colpitts, T.; O'quinn, B. Thin-film thermoelectric devices with high room-temperature figures of merit. *Nature* **2001**, *413*, 597.

(2) Venkatasubramanian, R. Lattice thermal conductivity reduction and phonon localizationlike behavior in superlattice structures. *Phys. Rev. B* **2000**, *61*, 3091−3097.

(3) Tang, X.; Xie, W.; Li, H.; Zhao, W.; Zhang, Q.; Niino, M. Preparation and thermoelectric transport properties of high-performance p-type Bi_2Te_3 with layered nanostructure. *Appl. Phys. Lett.* **2007**, *90*, No. 012102.

(4) Poudel, B.; Hao, Q.; Ma, Y.; Lan, Y.; Minnich, A.; Yu, B.; Yan, X.; Wang, D.; Muto, A.; Vashaee, D.; Chen, X.; Liu, J.; Dresselhaus, M. S.; Chen, G.; Ren, Z. High-Thermoelectric Performance of Nanostructured Bismuth Antimony Telluride Bulk Alloys. *Science* **2008**, *320*, 634−638.

(5) Cao, Y. Q.; Zhao, X. B.; Zhu, T. J.; Zhang, X. B.; Tu, J. P. Syntheses and thermoelectric properties of Bi_2Te_3/Sb_2Te_3 bulk nanocomposites with laminated nanostructure. *Appl. Phys. Lett.* **2008**, *92*, 143106.

(6) Zhou, J.; Jin, C.; Seol, J. H.; Li, X.; Shi, L. Thermoelectric properties of individual electrodeposited bismuth telluride nanowires. *Appl. Phys. Lett.* **2005**, *87*, 133109.

(7) Mavrokefalos, A.; Moore, A. L.; Pettes, M. T.; Shi, L.; Wang, W.; Li, X. Thermoelectric and structural characterizations of individual electrodeposited bismuth telluride nanowires. *J. Appl. Phys.* **2009**, *105*, 104318.

(8) Fang, H.; Feng, T.; Yang, H.; Ruan, X.; Wu, Y. Synthesis and thermoelectric properties of compositional-modulated lead telluride−bismuth telluride nanowire heterostructures. *Nano Lett.* **2013**, *13*, 2058−2063.

(9) Li, L.; Xu, S.; Li, G. Enhancement of thermoelectric properties in Bi−Sb−Te alloy nanowires by pulsed electrodeposition. *Energy Technol.* **2015**, *3*, 825−829.

(10) Khedim, M. B.; Cagnon, L.; Serradeil, V.; Fournier, T.; Bourgault, D. Thermoelectric nanowires based on bismuth telluride. *Mater. Today: Proc.* **2015**, *2*, 602−609.

(11) Ng, I. K.; Kok, K. Y.; Abd Rahman, C. Z. C.; Choo, T. F.; Saidin, N. U. Bismuth telluride based nanowires for thermoelectric power generation. *Mater. Today: Proc.* **2016**, *3*, 533−537.

(12) Hinsche, N. F.; Yavorsky, B. Y.; Gradhand, M.; Czerner, M.; Winkler, M.; König, J.; Böttner, H.; Mertig, I.; Zahn, P. Thermoelectric transport in Bi_2Te_3/Sb_2Te_3 superlattices. *Phys. Rev. B* **2012**, *86*, No. 085323.

(13) Böttner, H.; Chen, G.; Venkatasubramanian, R. Aspects of thin-film superlattice thermoelectric materials, devices, and applications. *MRS Bull.* **2006**, *31*, 211−217.

(14) Chowdhury, I.; Prasher, R.; Lofgreen, K.; Chrysler, G.; Narasimhan, S.; Mahajan, R.; Koester, D.; Alley, R.; Venkatasubramanian, R. On-chip cooling by superlattice-based thin-film thermoelectrics. *Nat. Nanotechnol.* **2009**, *4*, 235.

(15) Ju, S.; Shiga, T.; Feng, L.; Hou, Z.; Tsuda, K.; Shiomi, J. Designing Nanostructures for Phonon Transport via Bayesian Optimization. *Phys. Rev. X* **2017**, *7*, No. 021024.

(16) Seko, A.; Togo, A.; Hayashi, H.; Tsuda, K.; Chaput, L.; Tanaka, I. Prediction of Low-Thermal-Conductivity Compounds with First-Principles Anharmonic Lattice-Dynamics Calculations and Bayesian Optimization. *Phys. Rev. Lett.* **2015**, *115*, 205901.

(17) Zhang, H.; Minnich, A. J. The best nanoparticle size distribution for minimum thermal conductivity. *Sci. Rep.* **2015**, *5*, 8995.

(18) Yamawaki, M.; Ohnishi, M.; Ju, S.; Shiomi, J. Multifunctional structural design of graphene thermoelectrics by Bayesian optimization. *Sci. Adv.* **2018**, *4*, No. eaar4192.

(19) Chowdhury, P. R.; Reynolds, C.; Garrett, A.; Feng, T.; Adiga, S. P.; Ruan, X. Machine learning maximized Anderson localization of phonons in aperiodic superlattices. *Nano Energy* **2020**, *69*, 104428.

(20) Pattamatta, A.; Madnia, C. K. Modeling heat transfer in Bi2Te3−Sb2Te3 nanostructures. *Int. J. Heat Mass Transfer* **2009**, *52*, 860−869.
(21) Katcho, N. A.; Mingo, N.; Broido, D. A. Lattice thermal conductivity of $(Bi_{1-x}Sb_x)_2Te_3$ alloys with embedded nanoparticles. *Phys. Rev. B* **2012**, *85*, 115208.
(22) Qiu, B.; Ruan, X. Molecular dynamics simulations of lattice thermal conductivity of bismuth telluride using two-body interatomic potentials. *Phys. Rev. B* **2009**, *80*, 165203.
(23) Huang, B.-L.; Kaviany, M. Ab initio and molecular dynamics predictions for electron and phonon transport in bismuth telluride. *Phys. Rev. B* **2008**, *77*, 125209.
(24) Wang, Y.; Xu, X. Mode-Wise Phonon Properties of Bismuth Telluride. In *ASME 2012 International Mechanical Engineering Congress and Exposition*; American Society of Mechanical Engineers: 2012; pp. 2965−2969.
(25) Qiu, B.; Ruan, X. Thermal conductivity prediction and analysis of few-quintuple Bi_2Te_3 thin films: A molecular dynamics study. *Appl. Phys. Lett.* **2010**, *97*, 183107.
(26) Shao, C.; Bao, H. Thermal transport in bismuth telluride quintuple layer: mode-resolved phonon properties and substrate effects. *Sci. Rep.* **2016**, *6*, 27492.
(27) Zhang, J.; Liu, H. J.; Cheng, L.; Wei, J.; Shi, J.; Tang, X. F.; Uher, C. Enhanced thermoelectric performance of a quintuple layer of Bi2Te3. *J. Appl. Phys.* **2014**, *116*, No. 023706.
(28) Qiu, B.; Sun, L.; Ruan, X. Lattice thermal conductivity reduction in Bi_2Te_3 quantum wires with smooth and rough surfaces: A molecular dynamics study. *Phys. Rev. B* **2011**, *83*, No. 035312.
(29) Roy Chowdhury, P.; Feng, T.; Ruan, X. Development of interatomic potentials for the complex binary compound Sb_2Te_3 and the prediction of thermal conductivity. *Phys. Rev. B* **2019**, *99*, 155202.
(30) Lange, P. W. Ein Vergleich zwischen Bi2Te3 und Bi2Te2S. *Naturwissenschaften* **1939**, *27*, 133−134.
(31) Anderson, T. L.; Krause, H. B. Refinement of the Sb_2Te_3 and Sb_2Te_2Se structures and their relationship to nonstoichiometric $Sb_2Te_{3-y}Se_y$ compounds. *Acta Crystallogr., Sect. B: Struct. Crystallogr. Cryst. Chem.* **1974**, *30*, 1307−1310.
(32) Plimpton, S. Fast parallel algorithms for short-range molecular dynamics. *J. Comput. Phys.* **1995**, *117*, 1−19.
(33) Reddy, P.; Castelino, K.; Majumdar, A. Diffuse mismatch model of thermal boundary conductance using exact phonon dispersion. *Appl. Phys. Lett.* **2005**, *87*, 211908.
(34) Li, M.; Kang, J. S.; Nguyen, H. D.; Wu, H.; Aoki, T.; Hu, Y. Anisotropic thermal boundary resistance across 2D black phosphorus: Experiment and atomistic modeling of interfacial energy transport. *Adv. Mater.* **2019**, *31*, 1901021.
(35) Gale, J. D.; Rohl, A. L. The General Utility Lattice Program (GULP). *Mol. Simul.* **2003**, *29*, 291−341.
(36) Bessas, D.; Sergueev, I.; Wille, H.-C.; Perßon, J.; Ebling, D.; Hermann, R. P. Lattice dynamics in Bi_2Te_3 and Sb_2Te_3: Te and Sb density of phonon states. *Phys. Rev. B* **2012**, *86*, 224301.
(37) Feng, T.; Yao, W.; Wang, Z.; Shi, J.; Li, C.; Cao, B.; Ruan, X. Spectral analysis of nonequilibrium molecular dynamics: Spectral phonon temperature and local nonequilibrium in thin films and across interfaces. *Phys. Rev. B* **2017**, *95*, 195202.
(38) Feng, T.; Zhong, Y.; Shi, J.; Ruan, X. Unexpected high inelastic phonon transport across solid-solid interface: Modal nonequilibrium molecular dynamics simulations and Landauer analysis. *Phys. Rev. B* **2019**, *99*, No. 045301.
(39) Shi, J.; Yang, X.; Fisher, T. S.; Ruan, X. Dramatic increase in the thermal boundary conductance and radiation limit from a Non-equilibrium Landauer Approach. *arXiv:1812.07910* **2018**.
(40) Chalopin, Y.; Rajabpour, A.; Han, H.; Ni, Y.; Volz, S. Equilibrium molecular dynamics simulations on interfacial phonon transport. *Annu. Rev. Heat Transfer* **2014**, *17*, 147.
(41) Sääskilahti, K.; Oksanen, J.; Tulkki, J.; Volz, S. Role of anharmonic phonon scattering in the spectrally decomposed thermal conductance at planar interfaces. *Phys. Rev. B* **2014**, *90*, 134312.
(42) Gordiz, K.; Henry, A. A formalism for calculating the modal contributions to thermal interface conductance. *New J. Phys.* **2015**, *17*, 103002.
(43) Gordiz, K.; Henry, A. Phonon transport at crystalline Si/Ge interfaces: the role of interfacial modes of vibration. *Sci. Rep.* **2016**, *6*, 23139.
(44) Schelling, P. K.; Phillpot, S. R.; Keblinski, P. Comparison of atomic-level simulation methods for computing thermal conductivity. *Phys. Rev. B* **2002**, *65*, 144306.
(45) Borca-Tasciuc, T.; Liu, W.; Liu, J.; Zeng, T.; Song, D. W.; Moore, C. D.; Chen, G.; Wang, K. L.; Goorsky, M. S.; Radetic, T.; Gronsky, R.; Koga, T.; Dresselhaus, M. S. Thermal conductivity of symmetrically strained Si/Ge superlattices. *Superlattices Microstruct.* **2000**, *28*, 199−206.
(46) Saha, B.; Koh, Y. R.; Comparan, J.; Sadasivam, S.; Schroeder, J. L.; Garbrecht, M.; Mohammed, A.; Birch, J.; Fisher, T.; Shakouri, A.; Sands, T. D. Cross-plane thermal conductivity of (Ti,W)N/(Al,Sc)N metal/semiconductor superlattices. *Phys. Rev. B* **2016**, *93*, No. 045311.
(47) Chakraborty, S.; Kleint, C. A.; Heinrich, A.; Schneider, C. M.; Schumann, J.; Falke, M.; Teichert, S. Thermal conductivity in strain symmetrized Si/Ge superlattices on Si (111). *Appl. Phys. Lett.* **2003**, *83*, 4184−4186.
(48) Caylor, J. C.; Coonley, K.; Stuart, J.; Colpitts, T.; Venkatasubramanian, R. Enhanced thermoelectric performance in PbTe-based superlattice structures from reduction of lattice thermal conductivity. *Appl. Phys. Lett.* **2005**, *87*, No. 023105.
(49) Simkin, M. V.; Mahan, G. D. Minimum Thermal Conductivity of Superlattices. *Phys. Rev. Lett.* **2000**, *84*, 927−930.
(50) Daly, B. C.; Maris, H. J.; Imamura, K.; Tamura, S. Molecular dynamics calculation of the thermal conductivity of superlattices. *Phys. Rev. B* **2002**, *66*, No. 024301.
(51) Chen, Y.; Li, D.; Lukes, J. R.; Ni, Z.; Chen, M. Minimum superlattice thermal conductivity from molecular dynamics. *Phys. Rev. B* **2005**, *72*, 174302.
(52) Mizuno, H.; Mossa, S.; Barrat, J.-L. Beating the amorphous limit in thermal conductivity by superlattices design. *Sci. Rep.* **2015**, *5*, 14116.
(53) Termentzidis, K.; Chantrenne, P.; Duquesne, J.-Y.; Saci, A. Thermal conductivity of GaAs/AlAs superlattices and the puzzle of interfaces. *J. Phys.: Condens. Matter* **2010**, *22*, 475001.
(54) Chen, X.-K.; Xie, Z.-X.; Zhou, W.-X.; Tang, L.-M.; Chen, K.-Q. Phonon wave interference in graphene and boron nitride superlattice. *Appl. Phys. Lett.* **2016**, *109*, No. 023101.
(55) Hu, S.; Zhang, Z.; Jiang, P.; Chen, J.; Volz, S.; Nomura, M.; Li, B. Randomness-Induced Phonon Localization in Graphene Heat Conduction. *J. Phys. Chem. Lett.* **2018**, *9*, 3959−3968 PMID: 29968477.
(56) Felix, I. M.; Pereira, L. F. C. Thermal conductivity of graphene-hBN superlattice ribbons. *Sci. Rep.* **2018**, *8*, 2737.

https://dx.doi.org/10.1021/acsami.0c17851
ACS Appl. Mater. Interfaces 2021, 13, 4636−4642